



Title	Magnetic-field-sensing mechanism based on dual-vortex motion and magnetic noise
Author(s)	ZENG, T; Zhou, Y; Lin, KW; Lai, PT; Pong, PWT
Citation	Journal of Applied Physics, 2014, v. 115 n. 17, article no. 17D142, p. 17D142:1-3
Issued Date	2014
URL	http://hdl.handle.net/10722/200625
Rights	Copyright 2014 American Institute of Physics. This article may be downloaded for personal use only. Any other use requires prior permission of the author and the American Institute of Physics. The following article appeared in Journal of Applied Physics, 2014, v. 115 n. 17, article no. 17D142 and may be found at http://scitation.aip.org/content/aip/journal/jap/115/17/10.1063/1.4868603

Magnetic-field-sensing mechanism based on dual-vortex motion and magnetic noise

Tui Zeng, Yan Zhou, Ko-Wei Lin, Pui-To Lai, and Philip W. T. Pong

Citation: *Journal of Applied Physics* **115**, 17D142 (2014); doi: 10.1063/1.4868603

View online: <http://dx.doi.org/10.1063/1.4868603>

View Table of Contents: <http://scitation.aip.org/content/aip/journal/jap/115/17?ver=pdfcov>

Published by the [AIP Publishing](#)

Articles you may be interested in

[Stress reconfigurable tunable magnetoelectric resonators as magnetic sensors](#)

Appl. Phys. Lett. **102**, 042909 (2013); 10.1063/1.4789500

[Low noise dual free-layer magnetoresistive sensor with coupled resonance](#)

J. Appl. Phys. **105**, 07B708 (2009); 10.1063/1.3068644

[Thermal magnetization noise in submicrometer spin valve sensors](#)

J. Appl. Phys. **93**, 8576 (2003); 10.1063/1.1557853

[Temperature and field dependence of high-frequency magnetic noise in spin valve devices](#)

Appl. Phys. Lett. **82**, 91 (2003); 10.1063/1.1534386

[Designing a giant magnetoresistance field sensor via inferences from a giant magnetoresistance hysteresis model](#)

J. Appl. Phys. **87**, 5347 (2000); 10.1063/1.373343



Magnetic-field-sensing mechanism based on dual-vortex motion and magnetic noise

Tui Zeng,¹ Yan Zhou,^{2,a)} Ko-Wei Lin,³ Pui-To Lai,¹ and Philip W. T. Pong^{1,b)}

¹Department of Electrical and Electronic Engineering, The University of Hong Kong, Hong Kong

²Department of Physics, The University of Hong Kong, Hong Kong

³Department of Materials Science and Engineering, National Chung Hsing University, Taichung, Taiwan

(Presented 6 November 2013; received 23 September 2013; accepted 17 December 2013; published online 27 March 2014)

In this study, we report two novel field sensing mechanisms using elliptical permalloy single layer. Using micromagnetic modeling, dual-vortex structure is observed and stabilized in elliptical permalloy single layer by applying hard bias field (along the y-axis) and vertical axis field (perpendicular to plane). During the increasing or decreasing of the hard bias field within certain range, the dual vortices would move away from or approach to each other at a constant velocity, leading to a positive correlation between the hard bias field and the vortex gap. By exploring the magnetic noise properties of the elliptical permalloy single layer under various vortex gap, the vortex gap is found to be positively correlated with both the FMR (Ferromagnetic Resonance) peak positions and the integrated thermally excited mag-noise. Therefore, the combination of the dual-vortex motion and the magnetic noise properties make it possible to measure external field (along hard bias direction) through measuring the FMR peak positions or integrated thermally mag-noise. This FMR-peak-based field sensing mechanism and integrated-noise-based field sensing introduce a simple field sensor structure with expected highest sensitivity to 1.1%/Oe and field detectable range over 1000 Oe, which is promising for potential sensor applications. © 2014 AIP Publishing LLC. [<http://dx.doi.org/10.1063/1.4868603>]

I. INTRODUCTION

The vortex state, formed by the competition between the magnetostatic energy and exchange energy, is characterized by the closed flux domain structure. As one of the equilibrium configurations in micron- or submicron-sized ferromagnetic structures, the vortex state has been subject to intensive studies these years¹⁻⁴ and demonstrates potential technological implementation in racetrack memory.^{5,6} The manipulation of the vortex core motion by the external field can also open up the possibility of field sensing through measuring the vortex core motion properties, which is different from the typical GMR (Giant Magnetoresistance)/TMR (Tunneling Magnetoresistance) based field sensing mechanisms.

Utilizing micromagnetic simulation in this work, we explored explicitly how the dual-vortex motion is manipulated by the hard bias field. Furthermore, since the thermally excited magnetic noise which originates from thermal fluctuations^{7,8} has been shown to demonstrate a close connection with the vortex motion,⁹ the dependence of dual-vortex motion on the magnetic noise properties characterized by the FMR (Ferromagnetic Resonance) peak position and integrated thermally excited mag-noise is also studied in detail. Interestingly, by combining the results of the above two aspects, the magnetic noise properties can be related to the hard bias field through the dual-vortex motion, which makes the hard bias field sensing possible through measuring either the FMR peak positions or the integrated thermally excited mag-noise. The sensitivity and

the detectable range of these two novel field sensing mechanisms are fully investigated in this paper.

II. MICROMAGNETIC MODEL

Figure 1(a) shows the elliptical magnetic thin film structure in this study. The geometrical parameters are defined with long axis $L = 500$ nm, short axis $W = 200$ nm or 300 nm, and thickness $h = 50$ nm. The material is $\text{Ni}_{80}\text{Fe}_{20}$ with saturated magnetization $M_s = 860$ emu/cc, exchange constant $A_{ex} = 1.3 \times 10^{-6}$ ergs/cm, and magnetocrystalline anisotropy $K = 0$. The micromagnetic simulation was conducted with the OOMMF code.¹⁰ The simulation is carried out for the time period of 100 ns with the time step of 0.02 ps. The noise power

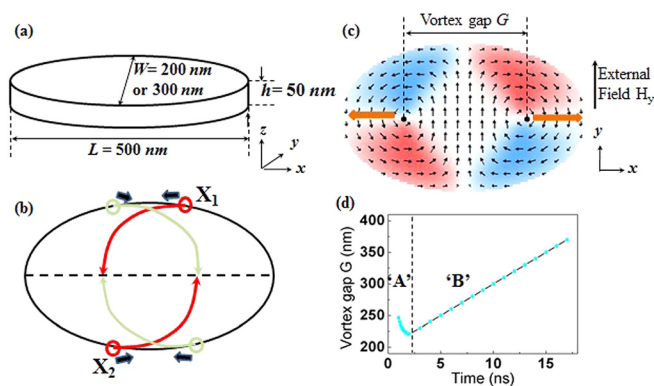


FIG. 1. (a) Schematics of the elliptical magnetic thin film structure. (b) Dual vortex formation process. The red lines and the olive green lines represent the trajectories of vortex cores. The black arrows represent the vortex motion direction. (c) Dual vortex and domain structure under hard bias field for elliptical magnetic layer with $500 \times 300 \times 50$ nm³ size. The orange arrows represent the vortex motion direction. (d) Time evolution of vortex gap.

^{a)}Electronic mail: yanzhou@hku.hk.

^{b)}Electronic mail: ppong@eee.hku.hk.

spectrum density (PSD) is calculated by the fast Fourier transform (FFT) from the time-dependent magnetization.

III. SIMULATION RESULTS

A. Dual vortex formation and thermally excited mag-noise

Previous investigation has already shown that sub-micron elliptical permalloy magnetic layer would only exhibit single vortex state or single domain structure under easy-axis bias field.¹¹ However, as the external field sweeps along the hard-axis direction, a dual vortex with opposite chirality configuration forms.¹² A relatively large bias field H_z (1000 Oe–5000 Oe) is applied perpendicular to the plane to ensure the stability of this dual vortex state.¹³ As shown in Fig. 1(b), the dual vortex cores X_1 and X_2 always first emerge at the elliptical edges in the 1st and 3rd quadrants, respectively, since demagnetization field in the edges is larger than the central part. Following different trajectories, the two vortex cores move to a stable state where both of them are located along the long axis symmetrically and simultaneously. Repeated hard-axis external field sweeping suggests another symmetric dual vortex formation process where the two vortex cores X_3 and X_4 first appear at the 2nd and 4th quadrants, respectively. Fig. 1(c) presents the stable dual vortex domain structure after this formation process. The vortex gap G is calculated as the hard bias field sweeps in Fig. 1(d). During the dual vortex formation stage “A,” the vortex gap rapidly decreases from 246 nm to 221 nm in 1 ns. During the vortex motion stage “B,” the two vortices move to opposite directions along the easy axis at a constant velocity.

During the sweeping process, the field range where the dual vortex motion occurs is defined as the detectable range. Within this field range, the magnetization along the hard axis M_y (not shown here) varies linearly with the hard-axis perpendicular field H_y in a reproducible manner. The detectable range under different perpendicular field H_z for cross section $500 \times 200 \text{ nm}^2$ and $500 \times 300 \text{ nm}^2$ was measured. Positive correlations are concluded between the detectable range and the hard-axis perpendicular field H_y for both cases. Meanwhile, it is found that the detectable range for relatively small area ($500 \times 200 \text{ nm}^2$) overwhelms that for large area ($500 \times 300 \text{ nm}^2$). This is because large cross-section area guarantees larger turn-up magnetization in the dual vortex cores compared to relatively small cross-section area, the demagnetization field in vortex cores of large cross section thus could overcome a relatively wide range of hard bias field H_y . With the perpendicular field H_z (such as 5000 Oe in Fig. 2), this phenomenon becomes even more obvious.

Fig. 3 demonstrates the thermally excited mag-noise PSDs under different hard bias fields H_y for elliptical cross-section areas of $500 \times 200 \text{ nm}^2$ and $500 \times 300 \text{ nm}^2$, respectively. The perpendicular field H_z is maintained at 5000 Oe where the maximum detectable range is obtained. Fig. 3(a) shows that major FMR peaks exist within the range from 1.21 GHz ($H_y = 100 \text{ Oe}$) to 2.2 GHz ($H_y = 1100 \text{ Oe}$). When H_y is over 700 Oe, minor peaks are observed from 2.98 GHz ($H_y = 700 \text{ Oe}$) to 4.74 GHz ($H_y = 1100 \text{ Oe}$). The low-frequency noise rises up significantly as H_y gradually increases.¹⁴ Meanwhile, the low-frequency PSD exhibits a $1/f$ tendency for $H_y = 900 \text{ Oe}$ and 1100 Oe. It is worth noting that

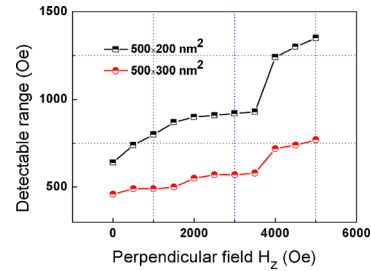


FIG. 2. The relation between detectable range of dual vortex state and perpendicular field H_z .

when $H_y = 500 \text{ Oe}$ and 700 Oe , multi-modes are activated around the major FMR peaks, which might be due to the oscillations in the vortex cores. Fig. 3(b) shows that major FMR peaks exist within the range from 1.35 GHz ($H_y = 100 \text{ Oe}$) to 1.82 GHz ($H_y = 700 \text{ Oe}$). Minor peaks are observed at 6.69 GHz ($H_y = 600 \text{ Oe}$) and 6.26 GHz ($H_y = 700 \text{ Oe}$). No $1/f$ tendency is observed in the low-frequency range.

B. Field sensing based on FMR major peak position

As shown in the PSDs in Fig. 3, there is correlation between the position of the major FMR peak and the hard bias field H_y . The positions of all the major FMR peaks for elliptical cross section of $500 \times 200 \text{ nm}^2$ and $500 \times 300 \text{ nm}^2$ and for perpendicular field $H_z = 2000 \text{ Oe}$ and 5000 Oe are calculated and displayed in Fig. 4(a). It is also noted that higher perpendicular field H_z (5000 Oe) or larger cross section results in FMR peaks at higher frequencies. In all cases, the frequency of FMR peak of the thermal mag-noise increases with the hard bias field H_y . The reproducible relation between FMR peak and hard bias field H_y renders a field-sensing mechanism. The magnitude of the hard-axis field H_y can be obtained by detecting the FMR peak in the PSD. The configuration of elliptical cross section of $500 \times 200 \text{ nm}^2$ and 5000 Oe perpendicular field H_z is found to provide the widest detectable range in this study. Approximately, we relate the FMR peak positions linearly to hard bias field within small hard bias field range (50 Oe here). The expected highest sensitivity could reach 0.17%/Oe when the elliptical cross section is $500 \times 200 \text{ nm}^2$ for a perpendicular field $H_z = 2000 \text{ Oe}$.

C. Field sensing based on integrated low-frequency mag-noise

By integrating the low-frequency thermally excited mag-noise PSDs from 0 to 2 GHz, the relation between the

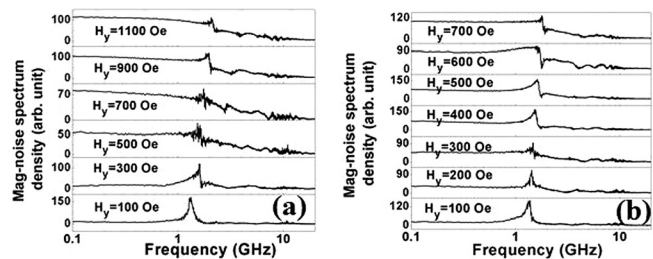


FIG. 3. Thermally excited mag-noise power spectrum density of dual vortex state under various hard bias fields H_y for (a) elliptical cross section of $500 \times 200 \text{ nm}^2$ and 5000 Oe perpendicular field H_z and (b) elliptical cross section of $500 \times 300 \text{ nm}^2$ and 5000 Oe perpendicular field H_z .

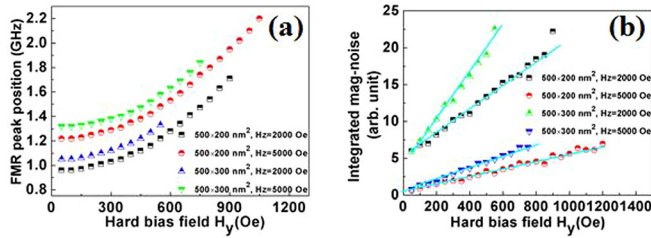


FIG. 4. (a) Dependence of FMR peak position on hard bias field H_y and (b) dependence of integrated mag-noise from 0–2 GHz on hard bias field H_y .

integrated low-frequency mag-noise and hard bias field H_y is obtained in Fig. 4(b). The integrated mag-noise correlates almost linearly with the hard bias field. This provides another field-sensing mechanism through detecting the integrated mag-noise. For an elliptical cross section of $500 \times 300 \text{ nm}^2$, the expected sensitivity increases from 0.56%/Oe to 1.1%/Oe as the perpendicular field H_z increases from 2000 Oe to 5000 Oe. For an elliptical cross section of $500 \times 200 \text{ nm}^2$, the expected sensitivity increases from 0.31%/Oe to 0.64%/Oe as the perpendicular field H_z increases from 2000 Oe to 5000 Oe. It can be observed that a stronger perpendicular field leads to the improvement in sensitivity. In addition, the increase of perpendicular field H_z would significantly suppress the mag-noise, which is conducive to the improvement of signal-to-noise ratio of the devices. It is suggested that the elliptical cross section with $500 \times 300 \text{ nm}^2$ and 5000 Oe perpendicular field provides the optimized configuration with relatively low mag-noise while maintaining highest sensitivity.

D. Comparison with conventional magnetoresistive sensors

The conventional GMR or TMR magnetic field sensors consist of multilayer thin films which require multiple sputtering sources. This kind of single-layer dual-vortex-based magnetic sensor would need one sputtering source, greatly simplifying the fabrication process and equipment. Fig. 5 shows the schematic illustration of this elliptical single-layer field sensor. As shown in Fig. 5(a), the hard bias axis of the sensor is configured along the external field in the x - y plane. The readout can be conducted through the electrodes connecting with the sensor. Fig. 5(b) shows the structure of the sensor and the electrodes in the x - z plane. The data of the FMR and the integrated mag-noise can be extracted from the noise analyzer.

Recently, GMR¹⁵ and TMR¹⁶ sensors have reached sensitivity level of around 6%/Oe and 10%/Oe, respectively, while their detectable range is less than 100 Oe. The large detectable range (higher than 1000 Oe) for the dual-vortex-based field sensing mechanisms becomes an obvious advantage, while it can provide a modest sensitivity of around 1.1%/Oe. There are no straight-forward means to manipulate the sensing range, sensitivity, and signal-to-noise ratio of GMR or TMR sensors without experimenting laboriously with different materials and fabrication parameters.^{17–19} The performance of this dual-vortex-based field sensing mechanism with a single elliptical magnetic layer, on the opposite, can be directly controlled through two parameters in a relatively predictable manner. Its sensing range can be varied by

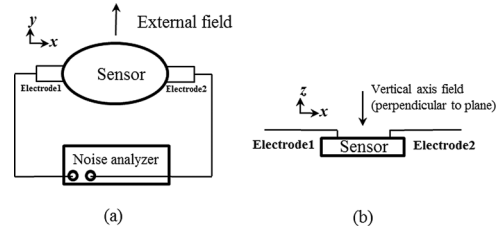


FIG. 5. Schematic illustration of the elliptical single layer field sensor in: (a) x - y plane; (b) x - z plane.

the short axis/long axis ratio while its sensitivity can be determined by both its short axis/long axis ratio and perpendicular bias field H_z . Its signal-to-noise ratio can be enhanced by increasing the perpendicular bias field H_z which suppresses the thermally excited mag-noise. Both the short axis/long axis ratio and perpendicular bias field H_z can be easily adjusted in the actual fabrication and application of the devices to achieve the desired sensing performance.

IV. CONCLUSIONS

In this paper, we explore the formation and the motion of dual vortex cores in elliptical magnetic layer at micron-level using micromagnetic simulation. FMR-peak-based field sensing mechanism and integrated-noise-based field sensing mechanism are proposed and studied. This dual-vortex-based approach offers the advantage over the traditional magnetoresistive magnetic field sensors that its sensing performance including sensing range, sensitivity, and signal-to-noise ratio can be easily controlled by varying the short axis/long axis ratio and perpendicular bias field H_z . Moreover, since it only involves a single layer, its fabrication process and equipment would be much simpler.

ACKNOWLEDGMENTS

This work was supported in part by the Seed Funding Program for Basic Research and Small Project Funding Program from the University of Hong Kong, ITF Tier 3 funding (ITS/112/12), RGC-GRF grant (HKU 704911 P), and University Grants Committee of Hong Kong (Contract No. AoE/P-04/08).

¹K.-S. Lee and S.-K. Kim, *Phys. Rev. B*, **78**, 014405 (2008).

²V. Uhlir *et al.*, *Nat. Nanotechnol.*, **8**, 341–346 (2013).

³K. Yamada *et al.*, *Appl. Phys. Lett.*, **96**, 192508 (2010).

⁴Y.-S. Yu *et al.*, *Sci. Rep.*, **3**, 1301 (2013).

⁵S. S. Parkin, M. Hayashi, and L. Thomas, *Science*, **320**, 190 (2008).

⁶S. Bohlens *et al.*, *Appl. Phys. Lett.*, **93**, 142508 (2008).

⁷N. Smith *et al.*, *IEEE Trans. Magn.*, **42**, 114–119 (2006).

⁸Y. Zhou, *IEEE Trans. Magn.*, **43**, 2187–2192 (2007).

⁹Y. Enomoto, *J. Phys.: Condens. Matter*, **9**, L239 (1997).

¹⁰M. J. Donahue and D. G. Porter, OOMMF user's guide, available from <http://math.nist.gov/oommf>.

¹¹F. Carace *et al.*, *Thin Solid Films*, **515**, 727–730 (2006).

¹²J. Lee *et al.*, *J. Magn. Magn. Mater.*, **272–276**, 736–737 (2004).

¹³T. Okuno, K. Mibu, and T. Shinjo, *J. Appl. Phys.*, **95**, 3612 (2004).

¹⁴Y. Guan *et al.*, *J. Appl. Phys.*, **105**, 07D127 (2009).

¹⁵P. Ripka, *IEEE Sens. J.*, **10**, 1108–1116 (2010).

¹⁶G. Q. Yu *et al.*, *J. Appl. Phys.*, **111**, 113906 (2012).

¹⁷W. F. Egelhoff *et al.*, *Sens. Actuators, A*, **155**, 217 (2009).

¹⁸W. F. Egelhoff, Jr. *et al.*, *J. Appl. Phys.*, **105**, 013921 (2009).

¹⁹Z. Q. Lei *et al.*, *IEEE Trans. Magn.*, **47**, 714 (2011).